Electronic Supplementary Information (ESI) for Mn-doped Co nanoparticles on wood-derived monolithic carbon for rechargeable zinc-air batteries

Lulu Zhang,[a] Yanyan Liu,*[,b,c] Shuling Liu,[a] Limin Zhou,[a] Xianli Wu,[a] Xianji Guo,*[,a] Anqi Zhang,[a] Pengxiang Zhang,[a] Baojun Li,[a] and Jianchun Jiang[c]

[a] Research Center of Green Catalysis, College of Chemistry, Zhengzhou University, 100 Science Road, Zhengzhou 450001, P R China

[b] College of Science, Henan Agricultural University, 63 Agriculture Road, Zhengzhou 450002, P R China

[c] Institute of Chemistry Industry of Forest Products, CAF, National Engineering Lab for Biomass Chemical Utilization, 16 Suojinwucun, Nanjing 210042, P R China

* Corresponding Authors E-mail: lyylhs180208@163.com (Y. Y. Liu), and guoxj@zzu.edu.cn (X. J. Guo)

Table of contents

Experimental details

1 Chemicals and materials

The wood samples were derived from the trunk of natural cedarwood. Cobalt (II) nitrate hexahydrate ($Co(NO_3)_2 \cdot 6H_2O$, ≥99%), zinc (II) nitrate hexahydrate ($Zn(NO_3)_2 \cdot 6H_2O$, ≥99%), manganese (II) acetate tetrahydrate ($Mn(Ac)_2 \cdot 4H_2O$, ≥98%), 2-methimidazole ($C_4H_6N_2$, ≥98%), methanol (CH_3OH, ≥99.7%), and ammonium chloride (NH_4Cl, ≥99.5%) were purchased from Aladdin. Ruthenium (IV) oxide (RuO_2, ≥99%), and platinum on carbon (Pt/C, 20 wt.% loading) were bought from Macklin. Deionized water (DI water, 18.2 MΩ cm) was used for all aqueous solutions. All chemicals were of analytical grade and used without further purification.

2 Material characterization

The morphologies of the samples were analyzed by SEM (ZEISS Sigma 500), TEM & EDS (FEI Tecnai G^2 F20 S-TWIN, 200 kV), and HAADF-STEM (JEM-ARM200F, 200 kV). The structures of the samples were characterized by XRD (Bruker D8 Advance with Cu K_α, λ = 1.5418 Å), nitrogen sorption isotherms (Micromeritic TriStar 3000, 77 K), Raman spectroscopy (Horiba Scientific LabRAM HR Evolution, 532 nm), and XPS (PHI quantera SXM spectrometer with Al K_α = 1486.6 eV). ICP-OES was recorded on Agilent 5110 instrument.

3 Electrochemical tests

All electrochemical measurements were finished on a CHI760E electrochemical workstation. The three-electrode system (Pine Instruments Co. Ltd., USA) includes a rotating disk electrode (RDE) or rotating ring-disk electrode (RRDE) modified with catalyst as the working electrode, a carbon rod as the counter electrode, and an Ag/AgCl electrode (filled with saturated KCl solution) as the reference. The working areas of RDE and RRDE are 0.196 and 0.247 cm^2, respectively. All catalysts were ground into powders for electrochemical tests. 4 mg catalyst and 50 μL Nafion (5 wt.%) were dispersed in 500 μL ethanol by ultrasonic for 30 min to prepare ink. 15 μL as-prepared ink was dropped on the glassy carbon of RDE/RRDE and dried at room temperature. All potentials were converted into reversible hydrogen electrode (RHE) by the following equation:

$$E_{vs.\,RHE} = E_{vs.\,Ag/AgCl} + 0.059pH + 0.197 \quad (1)$$

All catalysts were measured in O_2-saturated 0.1 M KOH solution for oxygen reduction reaction (ORR). Cyclic voltammetry (CV) tests were carried out in the voltage range of 0-1.2 V with a scan rate of 20 mV s^{-1}. The electrochemical active surface area was estimated by measuring double-layer capacitance (C_{dl}) in a non-Faradaic region from 1.05 to 1.15 V with different scan rates (20, 30, 40, 50, 60, and 70 mV s^{-1}). The value of C_{dl} was determined as the slope of a straight line from the plot of current density (half the sum of absolute values of current density at 1.10 V) against the scan rate. Linear sweep voltammetry (LSV) tests were employed with the scan rate of 5 mV s^{-1} and rotation speed from 400 to 2025 rpm. The accelerated durability test (ADT) was performed by 5000 cycles of the CV test from 1.0 to 0.7 V with a scan rate of 100 mV s^{-1}. Chronoamperometry (CP) tests were measured at 0.8 V for 20 h with a rotation speed of 800 rpm. For methanol resistance, the CP tests were recorded by adding 4 mL methanol into 100 mL electrolyte at the 400th second. Electrochemical impedance spectroscopy was tested in a frequency range from 10^6 to 10^{-1} Hz. The faradaic currents at the disk (I_D) and the ring (I_R) were determined by RRDE (platinum ring applied at 1.264 V). The peroxide yield (H_2O_2%) and electron-transfer number (n) were calculated according to the following equations:

$$[H_2O_2]\% = 200 \times \frac{I_R/N}{I_R/N + I_D} \quad (2)$$

$$n = 4 \times \frac{I_D}{I_R/N + I_D} \quad (3)$$

N is the collection efficiency of the platinum ring ($N = 0.41$).

The LSV tests for oxygen evolution reaction (OER) were carried out in N_2-saturated 0.1 M KOH solution from 0.864 to 1.764 V with a scan rate of 5 mV s^{-1}. CP tests were measured at 1.564 V for 20 h with a rotation speed of 800 rpm. Furthermore, commercial 20% Pt/C and RuO_2 were used as references for evaluating the electrocatalytic properties of various samples.

4 Assembly of liquid zinc-air batteries

The as-prepared ink was uniformly dispersed on hydrophobic carbon fiber and then dried at 60 °C for 2 h to obtain a new carbon fiber with the catalyst loading of 1.0 mg cm^{-2}.

A liquid zinc-air battery (ZABs) used a polished zinc plate (thickness of 0.8 mm) as the anode, an air electrode (consisting of gas diffusion layer on the air-facing side, nickel foam, and carbon fiber loaded with catalyst on the water-facing side) as the cathode, and a 6.0 M KOH

solution containing 0.2 M $Zn(OAc)_2$ as the electrolyte. The effective exposure area of the cathode to air is about 0.5 cm^2. Galvanostatic charge-discharge tests of ZABs were performed using an automated testing system (Neware CT-3008), and each discharge and charge period was set to be 20 min (discharge for 10 min and charge for 10 min). Discharge polarization curves were collected using LSV in the voltage range of 0-1.6 V with a scan rate of 5 mV s^{-1}. The energy density of ZABs was calculated from the applied current (I), the service hours (t), and the weight of consumed zinc (m_{Zn}):

$$Specific\ capacity = \frac{I \times t}{m_{Zn}} \quad (4)$$

5 Assembly of quasi-solid-state zinc-air batteries

Quasi-solid-state ZABs were established using zinc foil (thickness of 0.2 mm) as the anode, gel as the electrolyte, the prepared monolithic CoMn-N@NCW as the air cathode, and nickel foam as the current collector. The gel electrolyte was synthesized by solving, freezing, and thawing procedures. 3.0 g polyvinyl alcohol was dissolved in 30 mL DI water at 90 °C and stirred for 2 h to gain a transparent solution. 20 mL solution containing 0.2 M $Zn(Ac)_2$ and 6.0 M KOH was subsequently added into the above solution and stirred for 30 min. The obtained mixture was poured onto Petri dishes and frozen at -20 °C. The gel electrolyte was thawed at room temperature before use. The methods and conditions of tests were the same as those for liquid ZABs.

6 Supplementary figures and tables

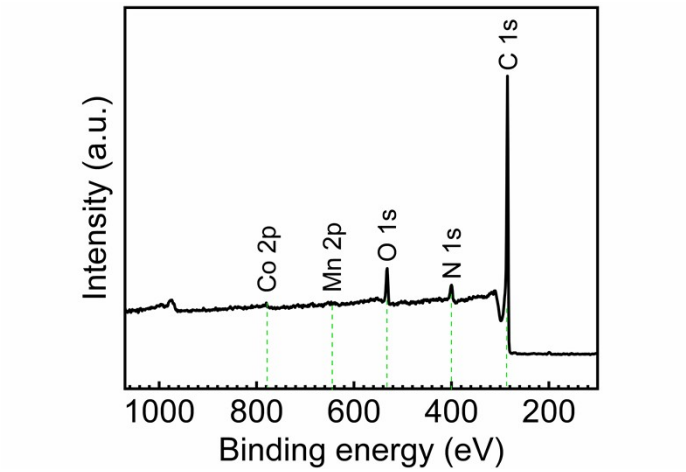

Fig. S1 XPS survey spectrum of CoMn-N@NCW.

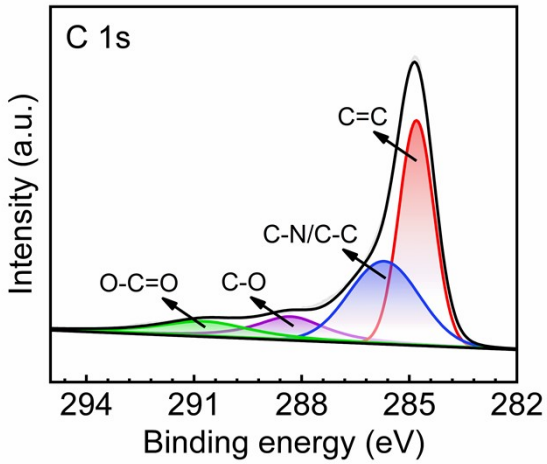

Fig. S2 The high-resolution C 1s spectrum of CoMn-N@NCW.

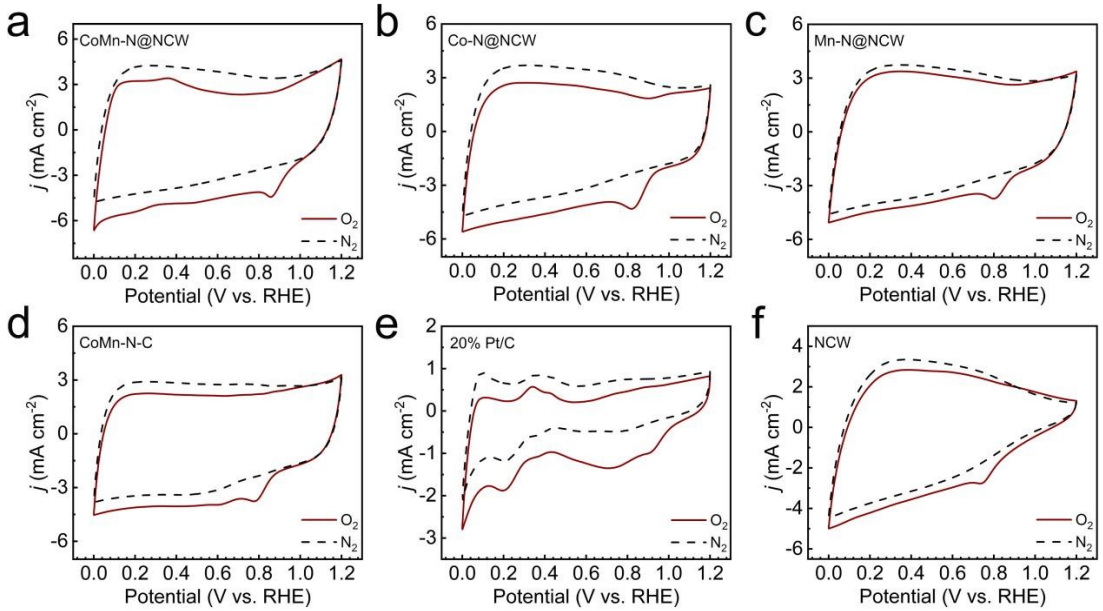

Fig. S3 CV curves of CoMn-N@NCW (a), Co-N@NCW (b), Mn-N@NCW (c), CoMn-N-C (d), 20% Pt/C (e), and NCW (f) in N_2- or O_2-saturated 0.1 M KOH solution.

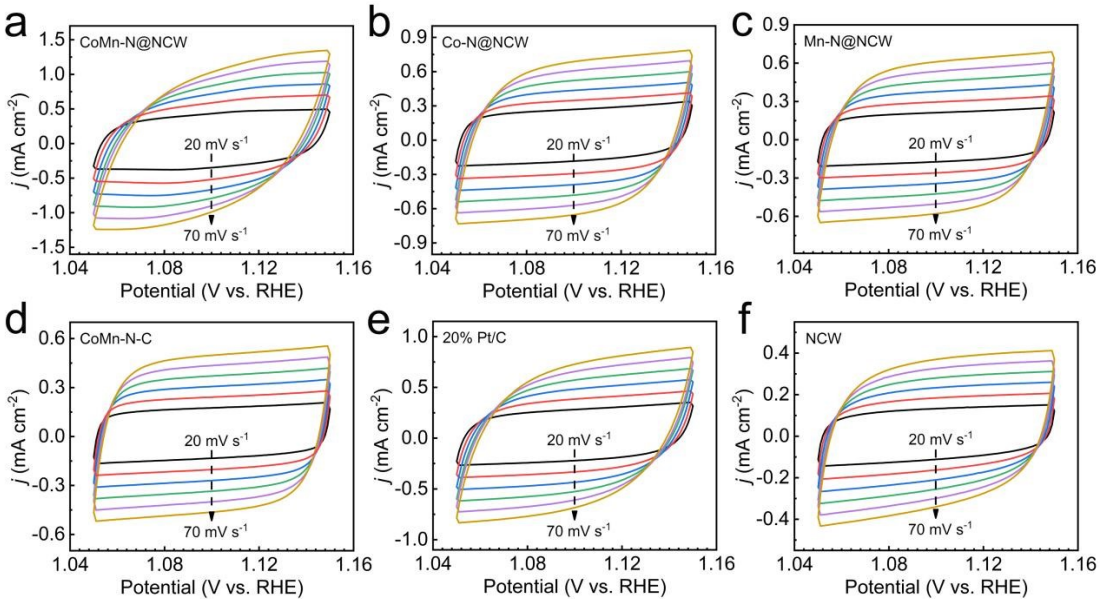

Fig. S4 CV curves of CoMn-N@NCW (a), Co-N@NCW (b), Mn-N@NCW (c), CoMn-N-C (d), 20% Pt/C (e), and NCW (f) at various scan rates from 20 to 70 mV s^{-1}.

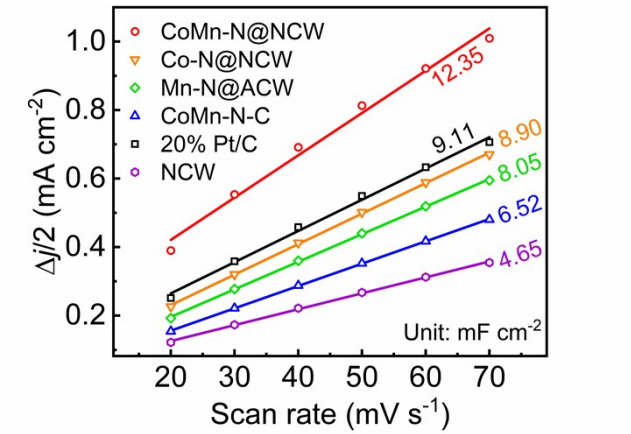

Fig. S5 The summarized C_{dl} of CoMn-N@NCW, Co-N@NCW, Mn-N@NCW, CoMn-N-C, 20% Pt/C, and NCW.

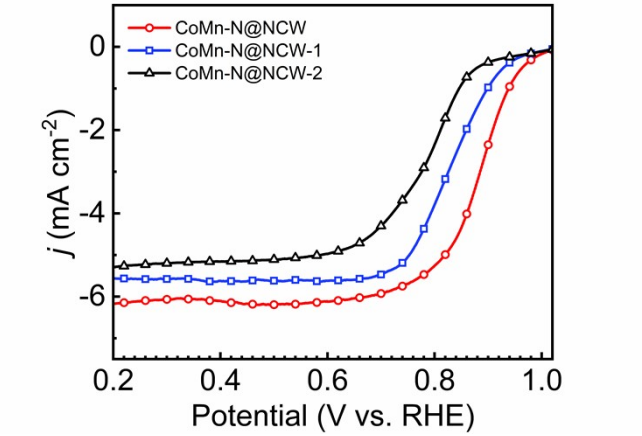

Fig. S6 ORR polarization curves for different masses of manganese salt.

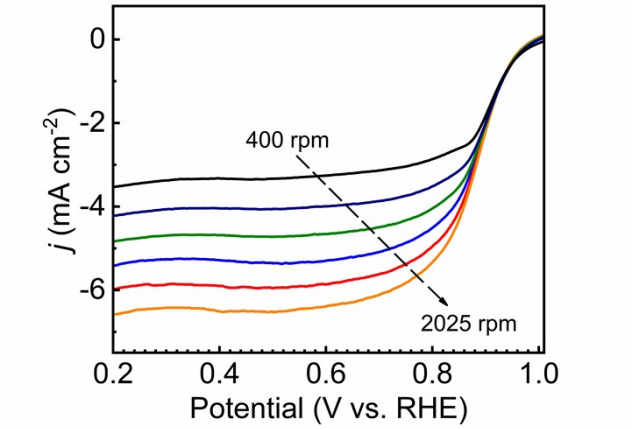

Fig. S7 ORR polarization curves of CoMn-N@NCW at different rotation speeds.

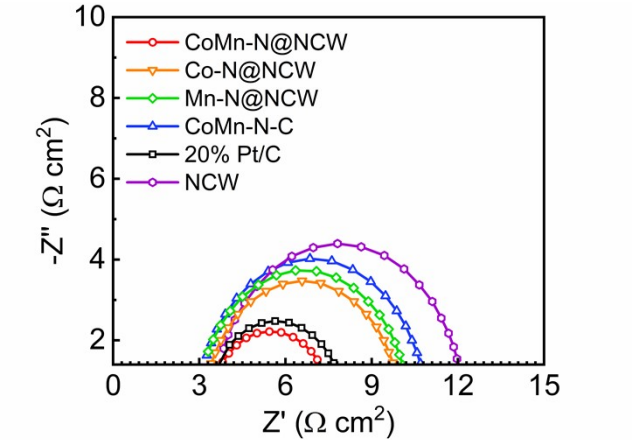

Fig. S8 Nyquist plots of CoMn-N@NCW, Co-N@NCW, Mn-N@NCW, CoMn-N-C, 20% Pt/C, and NCW.

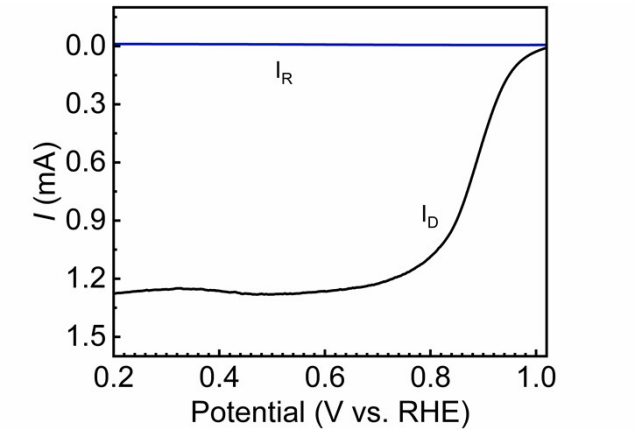

Fig. S9 I_D and I_R of CoMn-N@NCW.

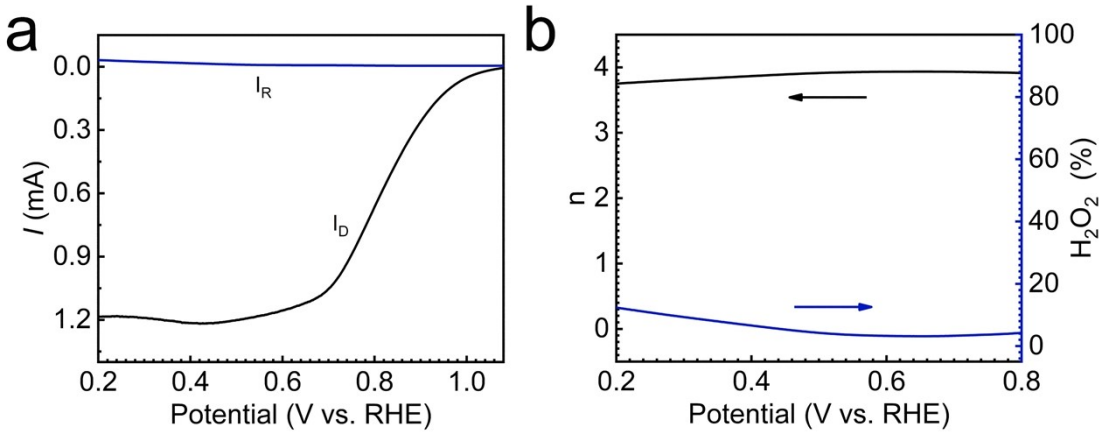

Fig. S10 (a) I_D and I_R of 20% Pt/C. (b) Calculated n and H_2O_2% of 20% Pt/C.

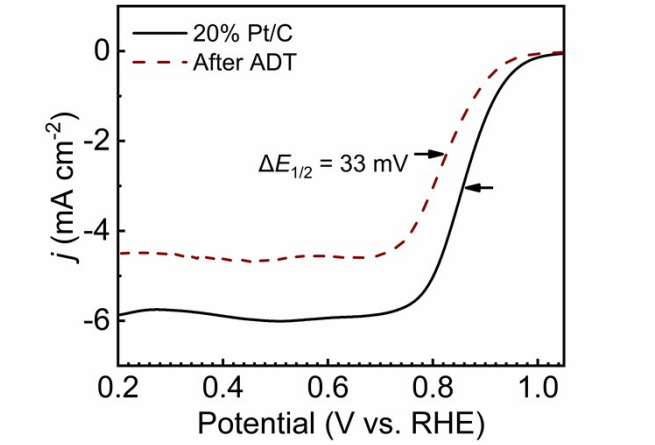

Fig. S11 LSV curves of 20% Pt/C before and after the ADT.

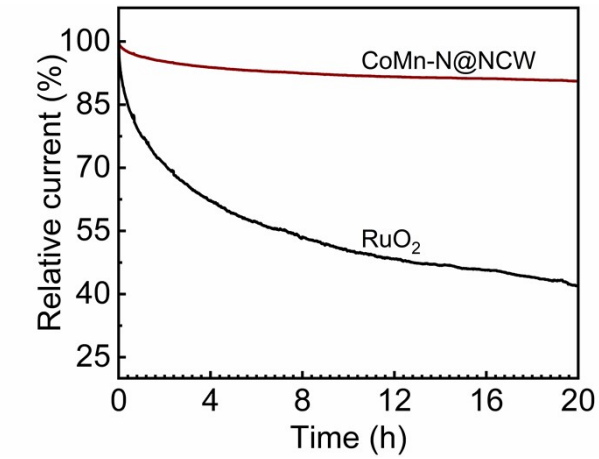

Fig. S12 CP tests of CoMn-N@NCW and RuO_2.

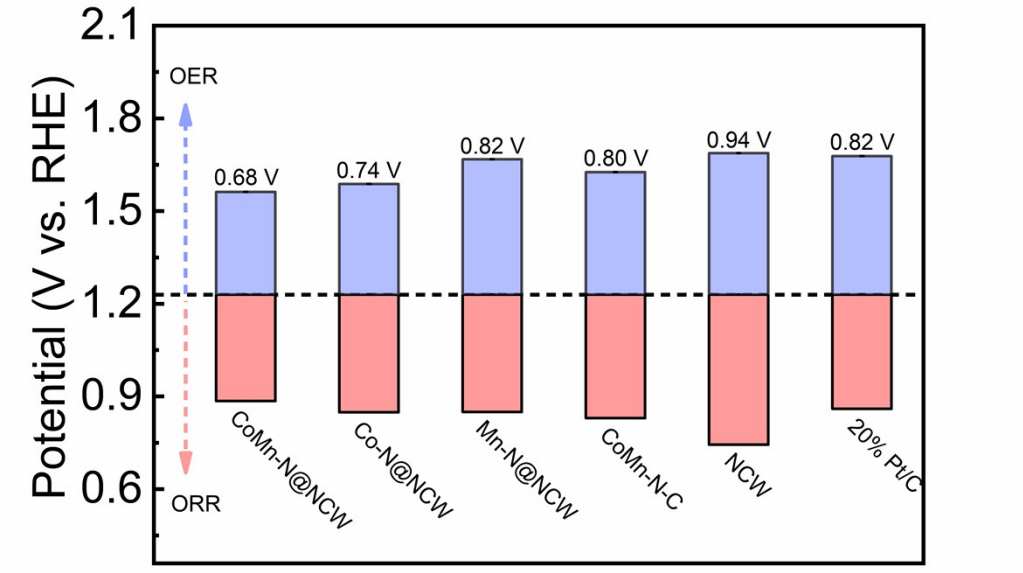

Fig. S13 ΔE of CoMn-N@NCW, Co-N@NCW, Mn-N@NCW, CoMn-N-C, NCW, and 20% Pt/C.

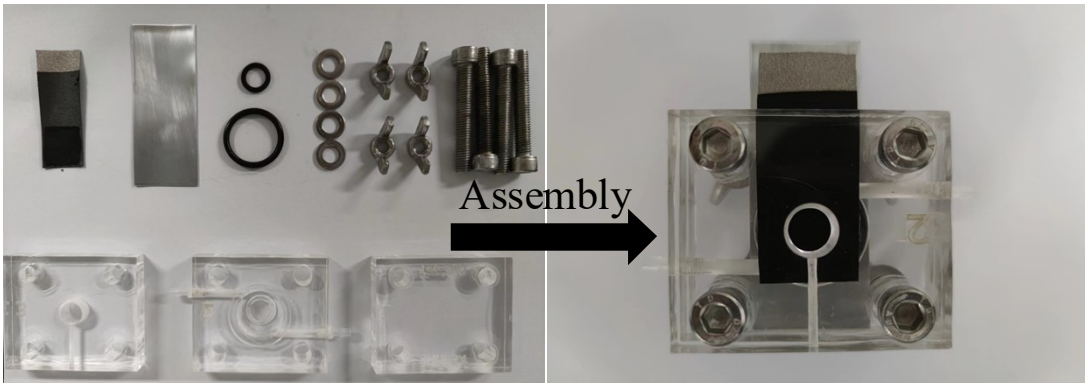

Fig. S14 Structure diagram of a liquid ZAB.

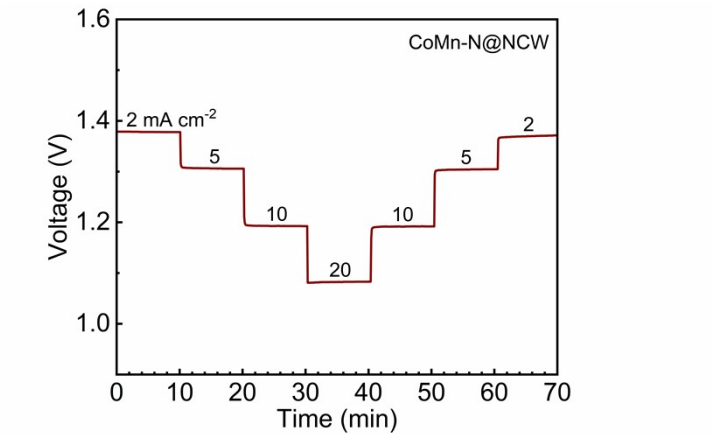

Fig. S15 Rate capability test of the ZAB with CoMn-N@NCW at different current densities.

Table S1 The element analysis result of CoMn-N@NCW determined by XPS.

Sample	C (at.%)	N (at.%)	O (at.%)	Co (at.%)	Mn (at.%)
CoMn-N@NCW	88.03	4.94	6.20	0.50	0.33

Table S2 The element analysis result of CoMn-N@NCW measured by ICP-OES.

Sample	Co (wt.%)	Mn (wt.%)
CoMn-N@NCW	1.33	0.44

Table S3 Comparison of ORR/OER activity and durability for ZABs in alkaline solutions with different Co-based catalysts.

Electrocatalyst	$E_{1/2,ORR}$ (V)	$E_{j=10,OER}$ (V)	ΔE (V) ($E_{j=10}$ - $E_{1/2}$)	Cycle	Reference
CoMn-N@NCW	**0.885**	**1.565**	**0.68**	**600 h**	**This work**
Co-CNHSC-3	0.84	1.58	0.74	80 h	1
NP-CoSANC	0.86	1.55	0.69	80 h	2
FeCoNC/SL	0.876	1.546	0.67	180 h	3
Co-CoN_4@NCNs	0.83	1.54	0.71	500 h	4
N/P-$Cu_{01}Co_{03}Mn_{06}O_2$/CNTs	0.82	1.52	0.70	200 h	5
V-Co_9S_8	0.83	1.61	0.78	420 h	6
15Co@Co_3O_4/PNC	0.89	1.58	0.69	200 h	7
CoNi/Co-N@HNC	0.86	1.58	0.72	350 h	8
FeCo-NC	0.877	1.579	0.702	190 h	9
Co_{NP}-Co_{SA}@DSCB	0.886	1.571	0.685	165 h	10

References

1 W. Zhang, X. M. Guo, C. Li, J. Y. Xue, W. Y. Xu, Z. Niu, H. W. Gu, C. Redshaw, J. P. Lang, *Carbon Energy*, 2023, **5**, e317.

2 J. Rong, E. Gao, N. C. Liu, W. Y. Chen, X. S. Rong, Y. Z. Zhang, X. D. Zheng, H. S. Ao, S. L. Xue, B. Huang, Z. Y. Li, F. X. Qiu, Y. T. Qian, *Energy Storage Mater.*, 2023, **56**, 165-173.

3 X. Zhao, J. B. Chen, Z. H. Bi, S. Q. Chen, L. G. Feng, X. H. Zhou, H. B. Zhang, Y. T. Zhou, T. Wågberg, G. Z. Hu, *Adv. Sci.*, 2023, **10**, 2205889.

4 K. X. Ding, J. G. Hu, J. Luo, L. M. Zhao, W. Jin, Y. P. Liu, Z. H. Wu, G. Q. Zou, H. S. Hou, X. B. Ji, *Adv. Funct. Mater.*, 2022, **32**, 2207331.

5 Y. Li, S. H. Talib, D. Q. Liu, K. Zong, A. Saad, Z. Q. Song, J. Zhao, W. Liu, F. D. Liu, Q. Q. Ji, P. Tsiakaras, X. K. Cai, *Appl. Catal. B Environ.*, 2023, **320**, 122023.

6 L. Wu, S. X. Li, L. X. Li, H. Zhang, L. Tao, X. Geng, H. M. Yang, W. M. Zhou, C. G. Sun, D. Y. Ju, B. G. An, *Appl. Catal. B Environ*., 2023, **324**, 122250.

7 W. Wu, R. Z. Chen, S. H. Chen, Z. C. Wang, N. C. Cheng, *Small*, 2023, **19**, 2300621.

8 Y. Y. Tan, Z. Y. Zhang, Z. Lei, L. Y. Yu, W. Wu, Z. C. Wang, N. C. Cheng, *Appl. Catal. B Environ.*, 2022, **304**, 121006.

9 Y. T. He, X. X. Yang, Y. S. Li, L. T. Liu, S. W. Guo, C. Y. Shu, F. Liu, Y. N. Liu, Q. Tan, G. Wu, *ACS Catal*., 2022, **12**, 1216.

10 J. Hong, M. S. Chen, L. Zhang, L. Qin, J. S. Hu, X. H. Huang, C. H. Zhou, Y. T. Zhou, T. Wågberg, G. Z. Hu, *Chem. Eng. J.*, 2023, **455**, 14040.